Melatonin delivered in solid lipid nanoparticles ameliorated its neuroprotective effects in cerebral ischemia

Saba Sohail [a,b,c], Fawad Ali Shah [a,d], Shahiq uz Zaman [a], Ali H. Almari [e], Imran Malik [a], Saifoor Ahmad Khan [f], Abir Abdullah Alamro [g], Alam Zeb [a,**], Fakhar ud Din [b,c,*]

[a] Riphah Institute of Pharmaceutical Sciences, Riphah International University, Islamabad, Pakistan
[b] Nanomedicine Research Group, Department of Pharmacy, Faculty of Biological Sciences, Quaid-i-Azam University, Islamabad, Pakistan
[c] Department of Pharmacy, Faculty of Biological Sciences, Quaid-i-Azam University, Islamabad, Pakistan
[d] Department of Pharmacology and Toxicology, College of Pharmacy, Prince Sattam Bin Abdulaziz University, Al-Kharj 11942, Saudi Arabia
[e] Department of Pharmaceutics, College of Pharmacy, King Khalid University, Abha 62529, Saudi Arabia
[f] Department of Community Medicine, Nowshera Medical College, Nowshera, Pakistan
[g] Department of Biochemistry, College of Science, King Saud University, Riyadh, Saudi Arabia

ARTICLE INFO

ABSTRACT

The current study explores the potential of melatonin (MLT)-loaded solid lipid nanoparticles (MLT-SLNs) for better neuroprotective effects in ischemic stroke. MLT-SLNs were prepared using lipid matrix of palmityl alcohol with a mixture of surfactants (Tween 40, Span 40, Myrj 52) for stabilizing the lipid matrix. MLT-SLNs were tested for physical and chemical properties, thermal and polymorphic changes, *in vitro* drug release and *in vivo* neuroprotective studies in rats using permanent middle cerebral artery occlusion (*p*-MCAO) model. The optimized MLT-SLNs showed particle size of ~159 nm, zeta potential of −29.6 mV and high entrapment efficiency ~92%. Thermal and polymorphic studies showed conversion of crystalline MLT to amorphous form after its entrapment in lipid matrix. MLT-SLNs displayed a sustained release pattern compared to MLT dispersion. MLT-SLNs significantly enhanced the neuroprotective profile of MLT ascertained by reduced brain infarction, recovered behavioral responses, low expression of inflammatory markers and improved oxidation protection in rats. MLT-SLNs also showed reduced hepatotoxicity compared to *p*-MCAO. From these outcomes, it is evidenced that MLT-SLNs have improved neuroprotection as compared to MLT dispersion and thereby present a promising approach to deliver MLT to the brain for better therapeutic outcomes in ischemic stroke.

1. Introduction

Stroke positions second in the world's leading causes of death, and is one of the major reasons for neurological impairment in adults. It has been estimated that almost 5 million persons die of stroke every year with another 5 million permanently disabled [1]. Ischemic and hemorrhagic strokes are the two main kinds of stroke accounting for 80% and 20% of cases, respectively. Ischemic stroke

is described by cell death in brain due to obstructed blood supply with a resultant deficient oxygen and nutrients delivery to maintain hemostasis, whereas hemorrhagic stroke is characterized by ruptured blood vessels in brain [1,2]. Tissue plasminogen activator is the only therapy authorized by the Food and Drug Administration (FDA) to open the clogged vessels in ischemic stroke [3]. However, thrombolytics such as *Activase®* and *Tenecteplase* are only effective when used within 3–4 h of ischemia, accompanied with possible side effects and increased risk of hemorrhage [4]. The investigational findings suggest that recanalization of clogged vessels is not adequate to manage ischemic injury, and neuroprotective treatments are more beneficial to hinder the development of cerebral ischemia by interfering biochemical pathways in ischemic cascade [5].

Melatonin (MLT) is an excellent neuroprotective agent amongst different endogenous and exogenous neuroprotective agents like estrogens and progesterone [6]. It is a hormone produced primarily by pineal gland and other tissues of the body such as gut, retina and glial cells. MLT is well-recognized for its potent anti-oxidant, anti-inflammatory properties and as a controller of circadian and seasonal phases. Its excellent safety profile, receptor-dependent and independent activities, and clinical applicability make it a preferred choice amongst neuroprotective compounds [7]. Neuroprotective properties of MLT in cerebral ischemia have been widely investigated in both *in vitro* and *in vivo* models. MLT decreases infarction volume, lessens brain water amount and increases neurological points in focal cerebral ischemic injury [8]. Despite of its excellent neuroprotective properties, MLT possesses some unfavorable biopharmaceutical properties such as poor water solubility (0.1 mg/mL, log P = 1.65) and thus it is classified as class II drug according to the Bio-pharmaceutics Classification System [9]. Therefore, bioavailability of MLT from conventional oral immediate-release dosage forms is quite low (~15%). In addition, MLT has a very small half-life of ~2 h, and oxidation susceptibility thereby restricting its therapeutic usage [10,11]. The neuroprotective effects of exogenously administered MLT in ischemic stroke could further be compromised because of relative impermeability of the blood-brain barrier (BBB) and limited brain accessibility. These drawbacks led the researchers to continuously explore new and effective delivery systems alongside new routes of administration to deliver a therapeutic meaningful concentration to brain. Several studies have reported different innovative nano-platforms for improved oral and intranasal delivery of MLT [12–16]. Among others nanocarriers, lipid-based nanoparticles have been widely investigated for penetrating the intact BBB [17–19] as well as bypassing the BBB via direct nose-to-brain delivery of various drugs [20–22]. MLT loaded in solid lipid nano-particles (SLNs) could provide promising approach for improving brain delivery and protecting it against potential enzymatic hydrolysis. SLNs offer benefits of increase drug entrapment, improved stability and biosafety, and sustained drug release opportunity [23].

Keeping in view the excellent neuroprotective effects of MLT and attractive features of SLNs, we explored the potential of MLT-SLNs for enhanced *in vivo* neuroprotective effects after intraperitoneal administration to rats in permanent middle artery occlusion (*p*-MCAO) stroke model. MLT-SLNs were prepared by using nanotemplate engineering procedure followed by their detailed characterization for physicochemical properties. The neuroprotective effects were assessed in terms of neurobehavioral score, infarct area, cerebral inflammation and degeneration.

2. Materials and methods

2.1. Materials

MLT, palmityl alcohol, Span 40, Tween 40, Tween 80, Myrj 52, and 2,3,4-triphenyltetrazolium chloride (TTC), reduced glutathione (GSH), 1-chlor-2,4-dinitrobenzene (CDNB), N-(1-Naphthyl) ethylenediamine dihydrochloride, trichloroacetic acid (TCA) and 5,50 -dithio-bis-(2- nitro benzoic acid; DTNB) were bought from Sigma Aldrich (St. Louis, MO, USA). NRf2 Elisa kit (Cat # SU-B30429), TNF- α Elisa kit (Cat # SU-B3098) p–NF–κB Elisa kit (Cat # SU-B28069) and HO-1 Elisa kit (Cat # SH-032529) were bought from Shanghai Yuchun Biotechnology, Co., Ltd. (Shanghai, China). All other chemicals were of analytical grade and used without further purification.

2.2. Method of preparation of MLT-SLNs

Nano-template engineering method was chosen to develop MLT-SLNs with minor alterations [23,24]. First of all, a mixture containing MLT, palmityl alcohol, Tween 40, Span 40 and Myrj 52 was heated in a water bath at 70 °C. Ten mL of deionized filtered water heated at 70 °C was then added to the molten mixture with continuous magnetic stirring at 800 rpm for 30 min to obtain a transparent nano-emulsion. This hot nanoemulsion was quickly chilled at 4 °C with continuous stirring to solidify the molten lipid and thus obtain MLT-SLNs. The resulting MLT-SLNs were passed through a 0.45 μm syringe filter to eliminate any larger masses and unentrapped free MLT. Till further analysis, MLT-SLNs were stored at 4 °C. Various lipids and surfactants were tested during preliminary studies for the preparation and optimization of MLT-SLNs (data not shown).

2.3. Characterization of MLT-SLNs

2.3.1. Particle size, polydispersity index (PDI), zeta potential and entrapment efficiency

A Zetasizer ZS-90 (Malvern Instruments; Malvern; Worcestershire; UK) was used to evaluate average particle size and PDI of MLT-SLNs [25]. MLT-SLNs were sufficiently diluted by using filtered deionized water, and particle size analysis was carried out at room temperature and a scattering angle of 90°. The entrapment efficiency and loading content of MLT-SLNs were determination by using indirect method [26]. Briefly, 2 mL of MLT-SLNs was centrifuged 13500 rpm at 4 °C for 30 min and the supernatant containing unentrapped free MLT was collected. The supernatant was diluted with ethanol and subjected to UV analysis (V-530; JASCO

Corporation; Tokyo; Japan) at wavelength of 278 nm for determining free MLT concentration. Finally, entrapment efficiency and loading content were calculated with the following formula:

$$\text{Entrapment efficiency } (\%) = \frac{\text{Weight of MLT entrapped in MLT} - \text{SLNs}}{\text{Total weight of MLT initially added}} \times 100$$

$$\text{Loading content } (\%) = \frac{\text{Weight of MLT entrapped in MLT} - \text{SLNs}}{\text{Total weight of MLT} - \text{SLNs}} \times 100$$

2.3.2. Transmission electron microscopy (TEM)

MLT-SLNs were visualized for surface morphology by using a transmission electron microscope (TEM, JEM-2100F, JEOL, Tokyo, Japan). One drop of MLT-SLNs was placed on a carbon-covered grid of 400-mesh and negatively stained with an aqueous solution of phosphotungstic acid (1%), dried at room temperature, and imaged with voltage of about 200 kV [27].

2.3.3. Differential scanning calorimetry (DSC)

Differential scanning calorimeter (DSC Q20; TA Instrument; New Castle; DE; USA) was used to investigate the melting pattern of lyophilized MLT-SLNs and their constituent solid ingredients. A freeze-dryer (TFD5503; IlShin BioBase Co., Ltd. Dongducheon, Republic of Korea) was used to lyophilize MLT-SLNs without using a cryoprotectant. For DSC study, approximately 5 mg of sample was heated in a regular aluminium pan at a rate of 10 $^{\circ}$C/min over the heating range of 0–150 °C.

2.3.4. Powder X-ray diffractometry (PXRD)

A powder X-ray diffractometer (D8 Advance-Bruker; Billerica; MA; USA) was employed to study the crystallinity of MLT-SLNs and their constituent solid ingredients). The instrument was operated over a 2θ range of 3–70° with scanning speed, current and voltage of 0.02°/sec, 40 mA and 40 kV, respectively.

2.3.5. Fourier transform infrared spectroscopy (FTIR)

Fourier transform infrared spectroscopy of MLT-SLNs was performed to study the compatibility between MLT and constituents of optimized SLNs. Using attenuated total reflectance fourier transform infrared spectrophotometer (FTIR, Eco Alpha II- Bruker, Billerica, MA, USA), spectra were obtained between 4000 and 400 cm^{-1} at a resolution of 4 cm^{-1}.

2.4. In vitro release of MLT from MLT-SLNs

In vitro drug release profile of MLT-SLNs was evaluated by utilizing dialysis bag diffusion technique in a USP dissolution type II-paddle apparatus (RC-8DS, Tianjin Guoming Medicinal, China) maintained at 37 °C and operated at 100 rpm. Dialysis membrane with molecular cut-off weight of 3500 Da (Spectrum Laboratories, Inc., Rancho Dominguez, CA, USA) was soaked for 15 min in the release medium before the analysis. Formulation containing 5 mg of MLT was added to dialysis membrane and immersed in 250 mL of phosphate buffer saline (pH 7.4) maintained at 37 ± 0.5 °C and magnetically stirred at 100 rpm. Because of low MLT solubility, sink condition was maintained by supplementing Tween 80 (0.5%, w/v) to the release medium. Two mL of samples were removed from the medium and an equivalent volume of fresh PBS was immediately added to maintain constant volume. The collected samples were examined for MLT contents by using UV–visible spectrophotometer at 278 nm.
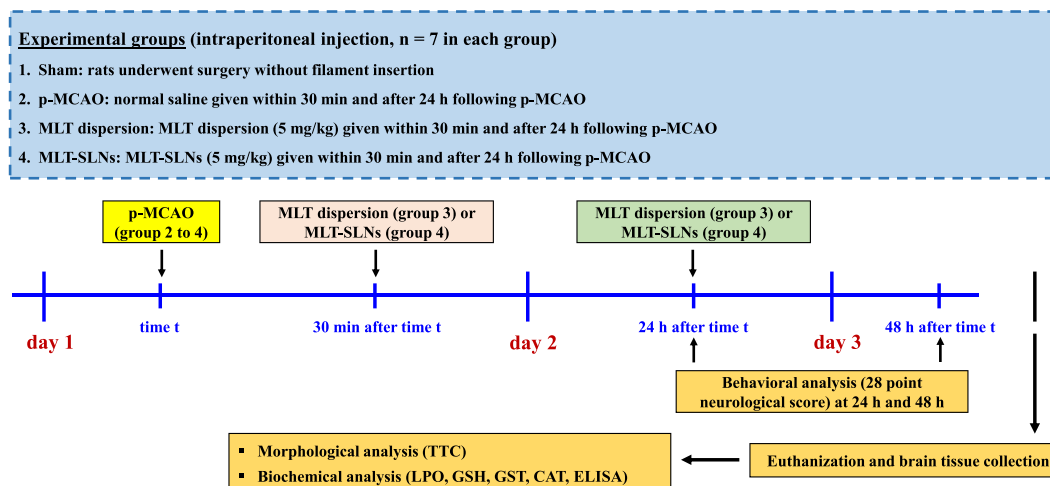
Fig. 1. Diagrammatic illustration of *in vivo* ischemic stroke model describing the experimental groups, their treatment timelines and different analyses carried out. Ischemic stroke was induced in rats by permanent middle cerebral artery occlusion (*p*-MCAO) technique.

2.5. Study design and MLT administration

Male Sprague Dawley rats (220–260 g) were housed in clean and standardized laboratory conditions and were given free access to food and water ad libitum. The institutional research and ethics committee of the Riphah Institute of Pharmaceutical Sciences, Islamabad, Pakistan, assessed and approved animal protocols according to NIH guidelines (Approval number: REC/RIPS/2019/12). The rats were randomly distributed into 4 groups (n = 7) named as sham, *p*-MCAO, MLT dispersion and MLT-SLNs groups. MLT dispersion in PBS (5 mg/kg) and MLT-SLNs (equivalent to 5 mg/kg) were intraperitoneally injected to respective groups within 30 min and 24 h after occlusion. Dose of MLT (5 mg/kg) was decided on the basis of its optimum neuroprotective effects in cerebral ischemia in a previous study [28]. Rats were decapitated after 48 h and brain were extracted and kept at −80 °C until used. One rat from sham and two each from *p*-MCAO, MLT dispersion and MLT-SLNs were died during surgical procedure and additional rats were used to make up the total number. The details of experimental groups and study design of *in vivo* ischemic stroke model are described Fig. 1.

2.6. p-MCAO procedure

p-MCAO in rats was carried out according to the previously published protocols [29,30]. A mixture of ketamine with xylazine (3.2:1, Intraperitoneal) was used to anesthetize rats. The common carotid and internal carotid artery were divided with a mid-line cervical opening without damaging Vagus nerve. The temporary suture was positioned around the common carotid artery and permanent suture (6/0 silk) was inserted around the external carotid artery. The internal carotid artery and pterygopalatine artery had a micro-vessel clip. The external carotid artery was incised and a filament of nylon (approximately 30 mm) with a sharp-edged tip was implanted. From the external carotid artery, a blue nylon filament was directed towards the internal carotid artery up to the starting point of middle cerebral artery before an obstruction was observed. After 48 h of permanent blockage, animals were killed and brain were extracted. Similar procedures were also carried out in sham group with an exception that nylon was not inserted.

2.7. Neurobehavioral test

The sensorimotor characteristics of rats were evaluated on a 28-point combined neurobehavioral score as described previously [28]. This scoring involved eleven tests including (1) motility (3 score), (2) righting (1 score), (3) horizontal bar (3 score), (4) general condition (3 score), (5) grip strength (2 score), (6) circling (4 score), (7) inclined platform (3 score), (8) contralateral rotation (2 score), (9) paw placement (4 score), (10) contralateral reflex (1 score), and (11) visual forepaw reaching (2 score). A composite score of 28 suggested good sensorimotor function, whereas 0 represented severe neurological damage.

2.8. TTC staining

Rats were decapitated under anesthesia after being tested for neurological deficits. Carefully separated brain tissues were washed with PBS and placed at −80 °C for few min. From the frontal lobe, brain slices (2 mm) were cut by utilizing a sharp edged blade and incubated in a 2% solution of 2,3,4-triphenyltetrazolium chloride (TTC) for approximately 20–30 min till complete differentiation was detected [31]. Paraformaldehyde solution (4%) was utilized to preserve the sections and placed at 4 °C till used. Brain sections were then snapped to measure and examine the infarcted area. The percentage infarction volume was measured using the ImageJ software. The following formula was used to measure the correct brain infarction: Corrected area of infarction = left area of the hemisphere – (right area of the hemisphere–area of infarction)/total area. The proportion of ischemic area was calculated using the following formula: area of infarction/complete section area × 100 [31].

2.9. ELISA

The concentration of nuclear factor erythroid 2-related factor 2 (NRf2), phosphorylated nuclear factor kappa B (*p*-NFκB), tumor necrosis factor-alpha (TNF-α) and hemeoxygenase-1 (HO-1) were examined by utilizing their respective rat kits. The brain slices were homogenized by homogenizer at 15,000 rpm, and the supernatant was collected after centrifugation (4000×*g*, 10 min). The whole protein quantity was measured by the bovine serum albumin protocol (Elabscience) and the equal protein amount was added to define the amount of NRf2, *p*-NFκB, TNF-α and HO-1 by utilizing microplate reader (BioTek; ELx808). Afterwards, final concentration in pico-gram/mL were normalized to whole protein concentration in pico-gram/mg of whole protein.

2.10. Lipid peroxidation (LPO) analysis

LPO analysis was performed to determine thiobarbituric acid reactive substances (TBARS) by utilizing fluorimetry. For this purpose, brain slices were homogenized in 20 mM of tromethamine-hydrochloride (10 mL, pH 7.4) at 4 °C by using homogenizer. The sample was centrifuged (1000×*g*) for 10 min at 4 °C and clear supernatant was collected. Ferric ammonium sulfate solution was added into 40 μL of supernatant and then incubated at 37 °C for approximately 30 min. Lastly, 75 μL of thiobarbituric acid was added to the mixture, measured with a microplate reader at 532 nm and displayed as TBARS-nM/min/mg of protein.

2.11. Oxidative enzymes assays

The concentration of oxidative stress markers such as glutathione s-transferase (GST) and reduced glutathione (GSH) were measured to evaluate oxidative injury in brain. The cerebral tissues dissolved in 0.1 M PBS (pH 7.4) containing protease inhibitor as phenylmethylsulfonyl fluoride (PMSF) were homogenized and centrifuged at $4000 \times g$ for 10 min at 4 °C and clear supernatant was collected. GSH concentration was measured utilizing a previously reported procedure with minor alterations [32]. Briefly, 0.6 mM 5, 50 -dithio-bis-(2- nitro benzoic acid) was added to 0.2 M sodium phosphate. Afterwards, two mL of that prepared solution were added to 0.2 mL of separated supernatant. Then 0.2 M solution of PBS was added again to make a total volume to 3 mL. The absorbance of prepared final solution was calculated at 412 nm by utilizing spectrophotometer. Phosphate buffer solution was taken as blank while 5, 50 -dithio-bis-(2- nitro benzoic acid) solution was taken as control. GSH concentration was stated in µmoles/mg of proteins. Similarly, GST activity was measured with a previously reported method [33]. Five mM GSH and 1 mM CDNB was added in solution of 0.1 M phosphate buffer. Three replica solutions of 1.2 mL of prepared mixture were then added to glass vials. Afterwards, separated supernatant of 60 µL was included to the designed mixture. Triplicate separate blanks were also prepared by utilizing 60 µL of water as an alternative of tissue lysate. Aliquots of 210 µL from the final mixture were then added in a microtiter plate and rate of reaction was noted at 340 nm for 5 min at 23 °C with help of microplate reader (BioTek ELx808; Winooski; VT; USA). GST concentration was measured by utilizing the extinction coefficient of the prepared mixture and presented as µmoles of (CDNB conjugate/min/mg) of protein.

2.12. Evaluation of ALT and AST levels in plasma

The liver function test was performed to find the hepatotoxicity of free MLT and MLT-SLNs. Rats plasma was used to determine enzymatic biomarkers such as aspartate aminotransferase (AST) and alanine aminotransferase (ALT) as indicators of liver function. Standardized test kits (Abnova Corporation) were used to analyze ALT and AST levels in plasma.

2.13. Statistical analysis

All data are presented as mean ± standard deviation. Data were statistically analyzed by either using a one-way or two-way analysis of variance followed by post-hoc Bonferroni multiple comparison tests at a significance level of less than 0.01 or 0.05. For this purpose, SigmaPlot software (version 14, Systat software Inc., Berkshire, UK) was used.

3. Results and discussion

3.1. Preparation of MLT-SLNs

Depending upon the solubility of drug, pre-emulsion type, ingredients biocompatibility and formulation stability, various lipids and surfactants were investigated to prepare and optimize MLT-SLNs. A 16-Carbon saturated fatty alcohol (palmityl alcohol) was chosen as
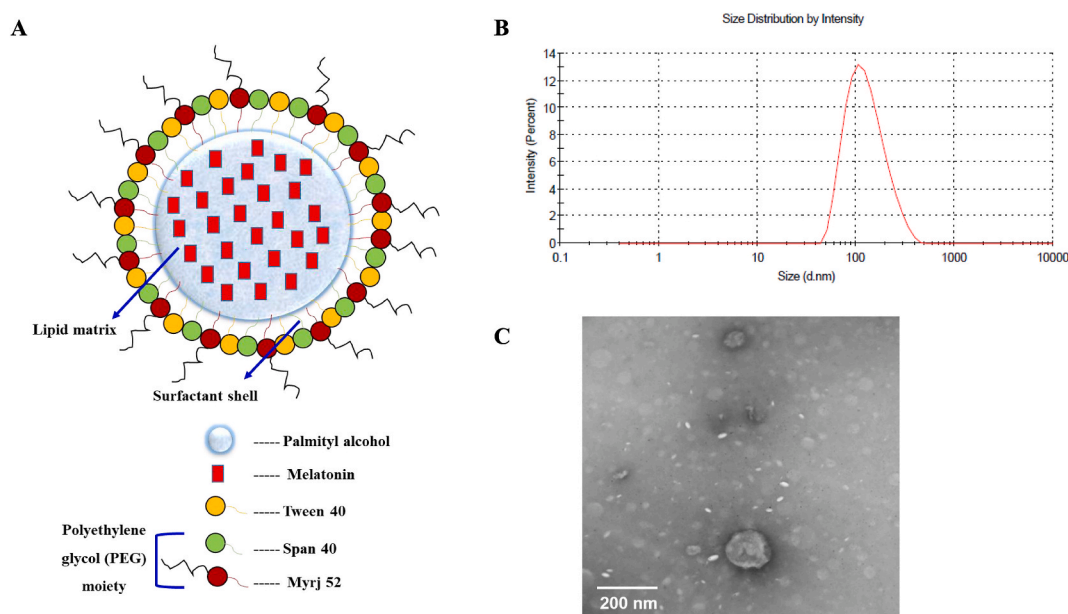
Fig. 2. Pictorial illustration (A); particle size (B); TEM analysis (C) of MLT-SLNs.

a lipid core of MLT-SLNs stabilized by a combination of surface active agents made up of Tween 40, Myrj 52 and Span 40. Palmityl alcohol is a safe, biocompatible and biodegradable solid lipid with a melting point of 49.3 °C. Solid lipids with above body temperature have robust lipophilic interactions with hydrophobic drugs, causing in increase entrapment efficiency and a stable core of lipid with sustained release pattern [34]. Furthermore, palmityl alcohol present in SLNs has been shown to be degraded and metabolized in the body through the enzyme endogenous alcohol dehydrogenase system [35]. The non-ionic surfactants Tween 40 and Span 40, with a palmitate entity in their structures were made a surfactant shell of miscible nature with a solid lipid core. Furthermore, Myrj 52 was applied to the surfactant mixture with large-chain polyoxyethylene (polyethylene glycol) moieties to serve as a steric stabilizer to increase the MLT-SLNs stability by decreasing superficial contacts among the particles. It has been stated that a mixture of surface active agents with vary HLB values appears to form the nano-emulsions with better stability than a use of single surface active agent [24].

In the case of cerebral distribution, lipid-prepared structure and minor mean size of SLNs can effectively pass the BBB, even without the surface incorporated with functional groups [36]. MLT-SLNs were successfully formed with good reproducibly by nano-template engineering technique. The procedure is an easy technique that does not require any organic solvents to prepare uniform nano-particles, or high-energy or pressure inputs [24]. The use of surface-active agents to stabilize the nanoparticles also based on hy-drophilic and lipophilic balance (HLB) of the prepared system that were composed of surfactants. The oil in water emulsions are efficiently stabilized by using the help of emulsifier that comprises HLB value of 8–18 [37]. The hydrophilic and lipophilic balance value of the surface active agent system must be close to that needed for a definite lipid to ensure optimum stability and performance [38]. For stabilizing the lipid core (HLB value = 15.5), the collective HLB of Tween 40; Myrj 52 and Span 40 was 15.9. MLT-SLNs were made up of drug, lipid (palmityl alcohol), surfactants (Tween 40, Span 40, Myrj 52) and filtered deionized water. Initial trials were performed to optimize SLN content concentrations, including 5–10 mg MLT, 10–15 mg palmityl alcohol, 15–20 mg Tween 40, 3–6.7 mg Span 40, 30–45 mg Myrj 52 and 10 ml distilled water. The particle size, PDI and zeta potential are essential features of SLNs to predict the physical stability. SLNs based formulations were optimized using various solid lipid and mixture of surfactant in weight ratios (data not shown) on basis of mean particle size; PDI; zeta potential and percent entrapment efficiency. Fig. 2A shows the structure of the MLT-SLNs. From all test formulations, the optimized formulation (composed of MLT; palmityl alcohol; Tween 40; Span 40 and Myrj 52 (weight ratio of 1/3/4/1.35/9) was selected an optimal MLT-SLNs having HLB value of 15.91, and proceeded to further characterization and further evaluated for *in vitro* drug release profile and *in vivo* neuroprotection, due to its most suitable particle size of 159.60 ± 15.9 nm, suitable PDI (0.255 ± 0.035), relatively high %EE (92.20 ± 0.96) and suitable zeta potential (−29.6 ± 5.9; Table 1).

3.2. Physico-chemical parameters and morphology of MLT-SLNs

The physical and chemical attributes of nanocarriers influence their skill to penetrate BBB in brain distribution. The mean particle size of MLT-SLNs was ~159 nm, PDI value of 0.255 showing homogeneous distribution of size. The mean size and PDI of MLT-SLNs were somewhat increased compared to blank SLNs (148.3 nm and 0.354). Nanoparticles showed permeation based on size through BBB with the minimum size nanoparticles being the best productive [39]. As expected, the produced SLNs have an mean size of fewer than 200 nm, creating them suitable for an increase-circulation time and an amplified resident time among the nanocarriers, raising the probability that the brain will take up these lipidic nanocarriers [40]. In fact, SLNs with a mean size between 120 and 200 nm will leak the reticuloendothelial system (RES) and thus avoid the filtration of the liver and spleen [41]. Low PDI (0.255) with unimodal distribution curve (Fig. 2B) display the homogeneous distribution of MLT-SLNs, since PDI value is less than 0.3 that usually specifies homogeneous particle size distribution. The MLT-SLNs displayed a surface with negative charged along with zeta potential values as − 29.6 ± 5.9 mV.

Zeta potential is the electrokinetic charge in dispersed colloidal particles that confirms the system stability. Zeta potential value of approximately −30 mV make an electro-repulsion in the system, and by preventing their aggregation, confirm the physical stability of nanocarriers. Furthermore, strongly negatively charged particles (−15 to −45 mV) in brain drug delivery are better to their positively charged counterparts, as they may threaten BBB's integrity [42]. The final optimized-MLT-SLNs presented increase value of drug incorporation efficiency (92.2 ± 0.96%) and loading content (5.2 ± 0.20%) which is beneficial for decreasing the injectable formu-lation administration volume and avoiding the bio-toxicity resulting from excessive excipient usage. The morphology of MLT-SLNs imaged by transmission electron microscope showed their spherical shape with smooth surface parallel to the homogeneous spreading of particles (Fig. 2C). The nanometric mean particle size of MLT-SLNs detected in the morphology was compatible with the findings gained by the zeta sizer results. MLT-SLN's spherical shape showing the smallest surface area with the least amount of surface-active agents needed for stabilization. The spherical shape of prepared SLNs can also characteristic to a delayed diffusion for

Table 1
Physicochemical properties of the optimized MLT-SLNs.

Physicochemical parameter	Blank SLNs	MLT-SLNs
Particle size (nm)	148.3 ± 11.6	159.6 ± 15.9
Polydispersity index (PDI)	0.354 ± 0.013	0.255 ± 0.035
Zeta potential (mV)	−21.4 ± 1.6	−29.6 ± 5.9
Incorporation efficiency (%, w/w)	–	92.2 ± 0.96

Data are expressed as mean ± S.D. (n = 3).

sustained release by minimizing the interaction with the environment [43].

3.3. Solid state characterization

The crystalline form and contact among lipid and MLT were measured by checking the heating pattern of MLT-SLNs and their separate components utilizing differential scanning calorimetry (Fig. 3A). The thermal curve of MLT (a) displayed a sharp endotherm peak at ~120 °C corresponding to the crystalline MLT melting point [13]. Similarly, palmityl alcohol thermal curve (b) displayed a sharp melting endotherm peak at ~52 °C suggesting its crystallinity. The characteristic endotherm peaks of Myrj 52 (c) were observed at ~51 °C [17]. The endothermic peak was wider when the content was formulated as SLNs, and the temperature was lower. This depression at the melting point can be due to the Kelvin effect [44]. The wider and depressed endothermic peak for SLNs could be owing to the nano-metric size of the particles that had an enormous surface area as well as impact of surface active agent [45]. The high endothermic peak of MLT has vanished in the thermogram of MLT-SLNs (d), suggesting the change of MLT inherent crystalline phase to amorphous phase after entrapment into lipid core [46,47]. It was also the likely findings that palmityl alcohol inhibited the MLT crystallization during SLNs preparation. Comparable investigations were testified by many research groups [44,48]. The amorphous behavior was supposed to have more energy with amplified surface area, improved solubility, bioavailability and dissolution [45]. The crystalline pattern of lyophilized MLT-SLNs was more evaluated by utilizing powder X-ray diffractometer (Fig. 3B). MLT's diffractogram pattern showed (a) sharp peaks at 2θ observed at 16.2°,16.46°, 17.8°,19.00°, 22.7°, 24.0°, 24.28°, 24.7°, 24.8°, 25.1°, 25.2°, 25.9°, 26.14° and 26.2° showing its presence in crystalline form [13]. Likewise, for palmityl alcohol, crystalline peaks were also detected at 21.1°, 22.3° and 25.3° (b). Degree of crystallinity was associated on the foundation of peak intensity. Myrj 52 displayed its peak at 19.12° and 23.32° (c). Though, the mentioned peaks of MLT-SLNs are broader with lesser intensities as compared to the palmityl alcohol, Myrj 52 and drug MLT. The findings propose that these nanoparticles have an amorphous form (d). This might be attributed to the robust association among hydrophobic drug and lipid core which suggests that MLT is fit incorporated in the SLNs and has an amorphous structure [10]. Additionally, the intensity of palmityl alcohol peaks in MLT-SLNs also decreased, indicating a reduction in solid lipid core crystallinity and a less well-ordered crystal structure. X-ray diffraction investigations are in consistent with the DSC findings which suggest an amorphous form of MLT in solid lipid core. This behavior is likely to increase the drug's solubility in water and in turn improved bioavailability [47].

FTIR study further investigated the molecular interactions of MLT with solid lipid core, and the infrared spectra formed in the scale of 4000-400 cm^{-1} is shown in Fig. 3C. Characteristic peaks of MLT (a) at 3303 cm^{-1} (N – H), 1629 cm^{-1} (C=O), 1555 cm^{-1} (C – O), and 1212 cm^{-1} (C – N) were observed [10]. Palmityl alcohol spectrum (b) displays five characteristic IR bands; the peaks were noted at about 2910 cm^{-1}, 2850 cm^{-1}, 1470 cm^{-1}, 1100 cm^{-1} and 717 cm^{-1}. The absorption peaks at 2910 cm^{-1} and 1100 cm^{-1} are the consequence of antisymmetric stretching vibration of – CH$_2$ group whereas the peak at 2850 cm^{-1} corresponds to the symmetric
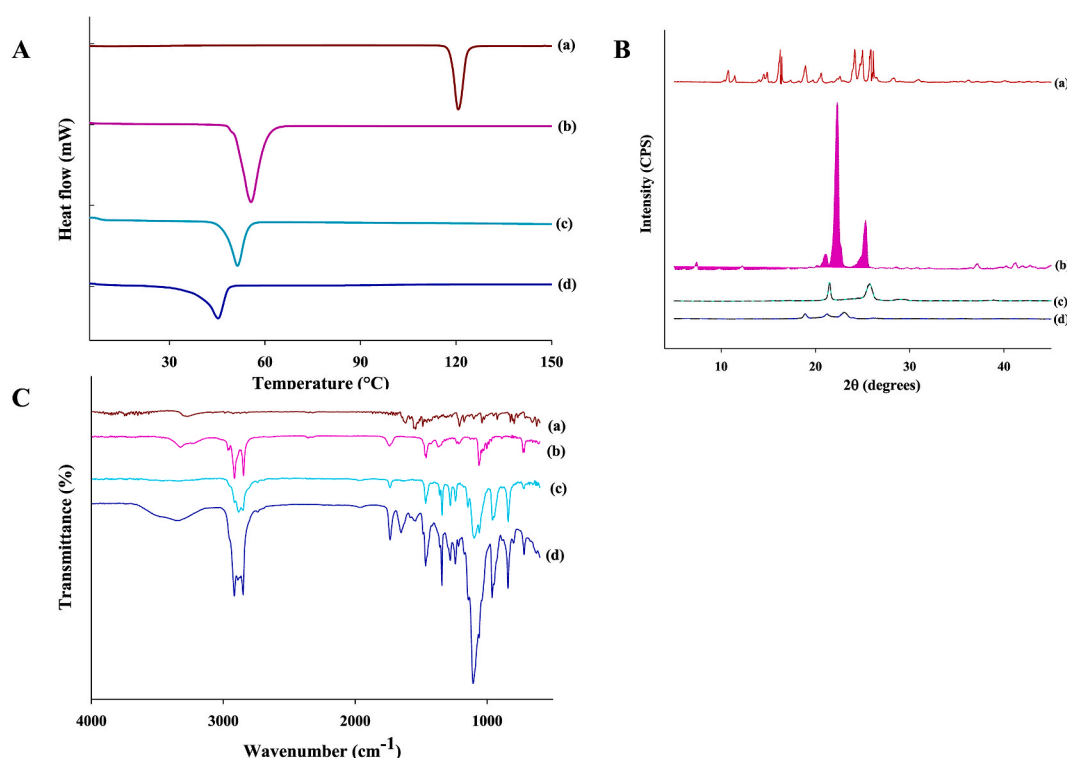
Fig. 3. DSC thermal curves (A); PXRD (B); and FTIR (C) of MLT (a), palmityl alcohol (b), Myrj 52 (c) and lyophilized MLT-SLNs (d).

stretching vibration of – CH$_2$ group [49]. Absorption peaks at 1470 cm^{-1} and 717 cm^{-1} reflect the rocking vibration of the group chain – (CH$_2$)$_4$. The infrared spectrum of Myrj-52 (c) presented principal peaks at 3600 cm^{-1} (–OH stretching), 1737 cm^{-1} (–C═O of ester), and 2893 cm^{-1} (–C–H stretching) [50]. The principal peaks of MLT were vanished in the spectrum for MLT-SLNs (d), representing the effective entrapment of MLT in the solid lipid core. The effective entrapment of MLT into MLT-SLN's lipid matrix showed the removal of its crystalline behavior as demonstrated by the absence of sharp peaks in DSC thermal curves; Powder X-ray diffraction investigations and infrared spectra obtained by FTIR analysis.

3.4. In vitro release pattern of MLT from MLT-SLNs

The *in vitro* release profile of MLT-SLNs was assessed in PBS (pH 7.4) and compared to that of MLT-dispersion. The findings of *in vitro* drug release are displayed in Fig. 4. MLT-SLNs reported ~22% of MLT release in the primary 2 h of PBS, followed by a slow and sustained release design with a total release of ~38% after duration of 24 h. Unlike the MLT-SLNs, the MLT dispersion displayed higher release with respectively 77% and 97% MLT released after 2 and 24 h. During the 24 h the analysis showed a biphasic pattern of sustained-release. The initial stage of burst-effect in 2 h is usually recognized to the rapid release of drug incorporated near the nanoparticles surface [10,51]. The surface-adhered drug spreads rapidly into the release medium, providing increase preliminary release rate [52]. Afterwards, MLT release was characterized by a slow and sustained drug release. After the primary stage, the slow-release pattern of MLT-SLNs may be attributed to the depth of entrapped MLT in the lipid core matrix of the MLT-SLNs and has an extended diffusion path to reach the surface associated to MLT incorporated near the surface and the barrier impact of the surfactant mixture shell [10,19,51]. The absence of profound burst release phenomena and continuous and prolonged MLT release for 24 h could be reasonably ascribed to drug-enriched core model. In contrary, drug-enriched shell model is described by drug deposition near the surface of SLNs with a significant burst release and much faster overall release rate. SLNs prepared with nano-template engineering technique have also shown similar release patterns in many other previous studies [23,24,53].

3.5. Effect of MLT-SLNs on neurological score and brain infarction

MLT-SLNs or MLT dispersion (dose = 5 mg/kg) were injected within 30 min and after 24 h of *p*-MCAO, and their effects on neurological score and brain infarction were assessed. Neurological scores were examined 24 h and 48 h after *p*-MCAO. Animals exposed to *p*-MCAO displayed significant neurological impairment reaching from spontaneous circling (scores = 3 and 4) to unconsciousness [54]. MLT dispersion treatment lessened these neurological scores, suggesting that MLT can reduce neurological impairment (p value < 0.05, Fig. 5A), but the best results were obtained for MLT-SLNs (p < 0.01) as compared to MLT-dispersion. Interestingly, on day 2 after *p*-MCAO, a substantial improvement in the cumulative neurological score was observed in rats treated with MLT dispersion and MLT-SLNs suggesting that after *p*-MCAO, a spontaneous sensorimotor functional recovery occurred. There was no obvious neurological function deficit in sham group, and the neurological scores were significantly decreased in *p*-MCAO. In this type of ischemic model, the neocortex, putamen and caudate were the major regularly injured areas [8]. Hence, TTC staining was done to access the cellular viability and neuronal damage, that completely defined the infarcted region from the profound red region of whole brain tissue (Fig. 5B), without infarction shown by sham-operated rats. MLT dispersion (26 ± 2%, p < 0.05) treatment decreased infarction size while MLT-SLNs substantially reduced *p*-MCAO-induced infarction region (8 ± 2%, p < 0.01) as compared to MLT dispersion (Fig. 5C). These results suggest improved brain distribution of MLT delivered in MLT-SLNs. The increased vascular permeability of the BBB around the ischemic area could further promote the delivery of MLT-SLNs [55]. Small particle size of SLNs (100–200 nm), increased surface area and lipophilic nature of MLT-SLNs could have contributed to increased residence period that facilitated their transfer into the cerebral cells by establishing drug-concentration gradient [56,57]. In addition, endocytosis, transcytosis and the opening of close-fitting junctions between the endothelial tissues could also facilitate drug and SLNs transport across
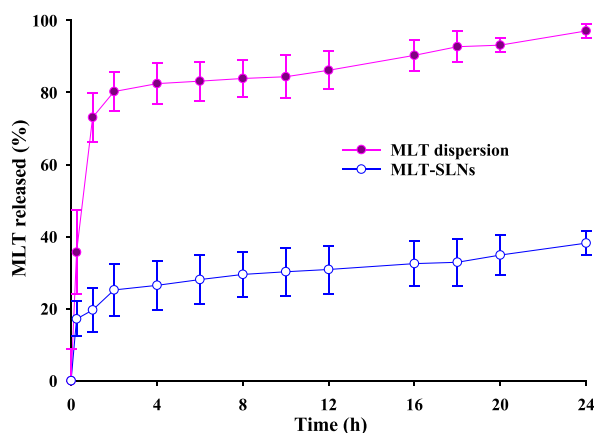
Fig. 4. *In vitro* release profile of MLT-SLNs evaluated in PBS at pH 7.4. Data are displayed as mean ± standard deviation (n = 3).
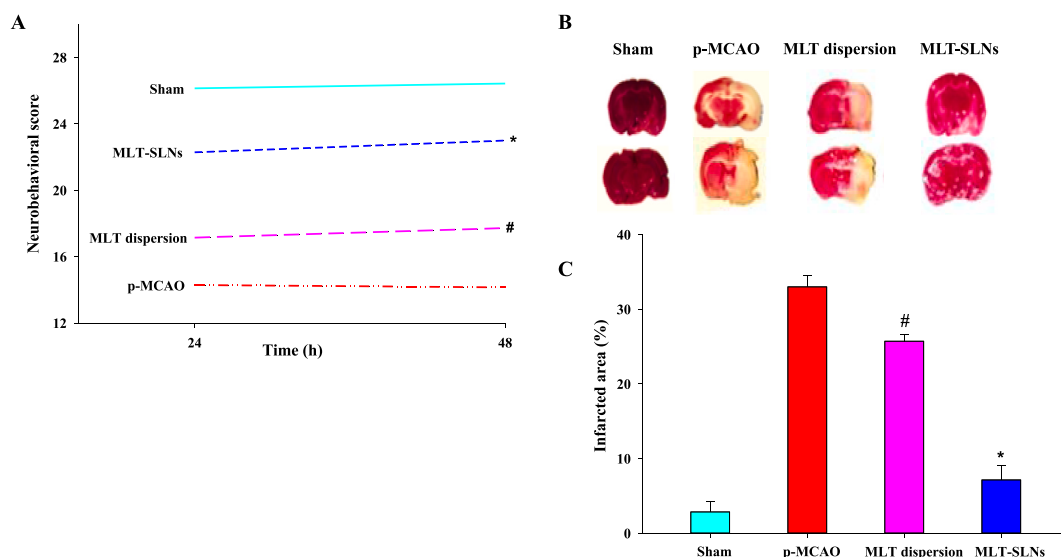
Fig. 5. Effects of MLT-SLNs against brain damage during ischemic stroke in rats: Neurobehavioral scores measured on 28 points composite scoring after 24 and 48 h of surgery (A), brain coronal sections stained with TTC (B) and brain infarction area measured from TTC-stained sections (C). Data are presented as mean ± standard deviation and statistically analyzed by either one-way (infarction) or two-way (neurobehavior) ANOVA (n = 7). *$p < 0.01$ against p-MCAO and MLT dispersion groups and #$p < 0.05$ against p-MCAO group.

the BBB [18,58]. Surfactants used in MLT-SLNs, particularly polysorbates (Tween 40 and Span 40) may produce membrane fluid-ization effect as well as inhibitory effects on efflux pumps in brain endothelial cells, thereby improving their brain delivery [56,59]. Studies have also revealed that polysorbates could facilitate adherence of apolipo protein E on the surface of SLNs, and these apoE-conjugated SLNs are likely to exploit receptor-mediated endocytosis pathway to enhance brain transport [57]. The collective contributions from these mechanisms could be ascribed to increased cerebral distribution of MLT-SLNs.

3.6. MLT-SLNs improved oxidative stress

The 2 interconnected pathophysiological procedures include inflammation and oxidative stress that are associated in brain ischemic injury and showed harmful effects till the recovery phase. Thiobarbituric acid reactive substances (TBARS) is a frequently process utilized to examine lipid peroxidation final product malondialdehyde; formed by lipid-peroxidation of polyunsaturated fatty-acids. We then carried out the thiobarbituric acid reactive substances assay and the findings displayed an extreme increased of lipid-peroxides in the permanent middle cerebral occlusion-operated rats, an outcome that might be saved by post-treatment of MLT-SLNs (Table 2). The lipid peroxidation concentration in the cortex homogenate was amplified to (117.0 ± 3.9) in the permanent-MCAO rats as associated to (59.0 ± 1.4) in the sham functioned rats. MLT-SLNs (5 mg/kg) significantly attenuated this increase (63.4 ± 0.9, p < 0.05) as compared to MLT-dispersion (82.2 ± 8.4), and further MLT-SLNs results are at a level equivalent to that of sham functioned group. Oxidative stress has a well-established role in cerebral injury [60]. A therapeutic approach with an antioxidant outcome may therefore be measured an effective method. MLT therapy at a dosage of 5 mg/kg decreased oxidative stress, and this was consistent to earlier results [61]. Possibly, we found that multiple oxidative damage factors are the essential factors in ischemic brain insult, causing a substantial upsurge in lipid peroxidation and protein oxidation followed by severe reduction in reduced glutathione and glutathione s-transferase and catalase. Consequently, we measured an increased level of TBARS, followed by exhausted rates of reduced gluta-thione, glutathione s-transferase and catalase in permanent-MCAO group while after treatment with MLT-SLNs effectively reversed these effects as compared to MLT dispersion, which is consistent with earlier findings where these antioxidants were utilized as a therapy in investigational ischemic stroke induced models [62]. Therefore, MLT-SLNs can effectively overwhelm oxidative damage and inflammatory reactions as compared to MLT dispersion by hunting free radicals and stopping lipid and protein peroxidation. MLT-SLNs significantly restored the antioxidants defense system (GSH, GST, CAT) and significantly attenuated MDA levels by inhibiting the lipid peroxidation in brain demonstrating neuroprotection against cerebral ischemia [63]. Free MLT have limited access to brain and may exhaust their antioxidant power before reaching the brain. MLT incorporation into SLNs could instead effectively increase brain localization and ROS scavenging activity by protecting them from undesired lipid and protein oxidation from the extracellular environment. Finally, the enhanced neuroprotective outcome of MLT-SLNs could be partly recognized to its enhanced anti-oxidant potential due to enhanced brain delivery of MLT-SLNs and in agreement to neurological score and brain infarction results.

3.7. MLT-SLNs enhanced the antioxidant enzymes

Nuclear factor erythroid 2-related factor 2 (NRf2) is an endogenously antioxidant marker that performs dynamic defensive

Table 2

Effects of MLT-SLNs on the concentration of oxidative enzymes in rats brain.

Groups	LPO (TBARS- nM/min/mg of protein)	GSH (μmoles/mg of protein)	GST (μmoles CDNB conjugate/min/mg of protein)	Catalase (μmoles H_2O_2/min/mg of protein)
Sham	59.0 ± 1.4	67.8 ± 2.8	21.6 ± 1.6	34.8 ± 1.6
p-MCAO	117.0 ± 3.9	12.4 ± 1.6	4.3 ± 0.8	3.2 ± 1.0
MLT dispersion	82.2 ± 8.4**	53.8 ± 3.1**	13.8 ± 1.6*	26.3 ± 1.5*
MLT-SLNs	63.4 ± 0.9**,#	63.6 ± 2.0**,#	18.2 ± 1.5**	30.3 ± 1.3**

Abbreviations: LPO; lipid peroxidation, TBARS; thiobarbituric acid reactive substances, GSH; reduced glutathione, GST; glutathione S-transferase, CDNB; 1-chlor- 2,4-dinitrobenzene, H_2O_2; hydrogen peroxide.

Data are presented as mean $\pm$ S.D. (n = 3) and analyzed by one-way ANOVA followed by post-hoc Bonferroni multiple comparison test using sigmaplot software (version 14). *$p < 0.05$ and **$p < 0.01$ against p-MCAO, whereas #$p < 0.05$ against MLT dispersion.

purposes [64]. Transfer of NRf2 to nucleus reproduces transcription of numerous late antioxidant proteins like superoxide dismutase (SOD), heme oxygenase-1 (HO-1) and reduced glutathione to defeat reactive oxygen species and defend the cells from apoptosis and neuroinflammation [65]. NRf2 also inhibited the levels of pro-inflammatory factors such as phospho nuclear factor kappa B and cyclooxygenase-2. Therefore, to observe impact of MLT-SLNs on NRf2 associated antioxidant signaling-pathways and proinflammatory markers, we calculated their values. Enzyme linked immunosorbent assay findings showed in Fig. 6 that NRf2 expression was enlarged in the permanent-MCAO rats as contrast to sham, while MLT-SLNs treatment significantly increases their expression as compared to MLT dispersion ($p < 0.05$). On the other hand, NRf2-lacking animals are strangely more liable to cerebral injury and neurological impairment as compared to wild type mice [65]. Our results confirmed the transfer of NRf2 from cytoplasm to nucleus in the permanent middle cerebral occlusion rats in reply to the oxidative stress indicators, as it our natural protective barrier. Though, an additional stimulation of NRf2 values was detected by providing MLT-SLNs, linked with increased levels of downstream markers HO-1, representing the significant anti-oxidant ability of MLT-SLNs. These findings indicated that MLT-SLNs could control both NRf2 and HO-1 appearance. NRf2 is a universally showed transcription marker that performs essential protective purposes by controlling the appearance of several detoxifying and antioxidant method-related proteins. The antioxidant signaling pathway NRf2 is one of the best powerful activated antioxidant pathways in laboratory and clinical trial studies during cerebral ischemia/reperfusion [66]. This is not the first research to prove MLT has an effect on NRf2 expression. Previously it was discovered that MLT therapy resulted in an increased protein expression of NRf2 in the nucleus and cytoplasm, thus exerting a potentially hepatoprotective effect against hepatic failure [67]. It was also stated that MLT triggered the antioxidant mechanism that depends on NRf2 and attenuated neuroinflammation induced by ethanol [68]. The findings of our current research have proposed that the expression of NRf2 increased significantly in treatment with MLT-SLNs ($p < 0.05$) as compared to MLT dispersion. These results further suggested that the oxidative stress caused by reactive oxygen species was lessened by the significant stimulation of the endogenous antioxidant NRf2/HO-1 by the MLT-SLNs treatment as compared to MLT-dispersion. Moreover, how MLT-SLNs effects NRf2 translocation needs further investigation. Likewise, HO-1, GST and reduced glutathione displayed a comparable design of alterations. *p*-MCAO caused an increase in reactive oxygen species, related with reduction of reduced glutathione levels (12.4 ± 1.6), GST activity (4.3 ± 0.8), and catalase (3.2 ± 1.0) in the brain cortical tissue. MLT-SLNs treatment weakened significantly downregulation of GSH (63.6 ± 2, $p < 0.01$), GST (18.2 ± 1.5, $p < 0.01$), and catalase (30.3 ± 1.3, $p < 0.01$) as related to MLT-dispersion GSH (53.8 ± 3.1, $p < 0.01$), GST (13.8 ± 1.6, $p < 0.05$), and catalase (26.3 ± 1.5, $p < 0.05$), and further MLT-SLNs results were comparable to the sham operated group. As mentioned, reduced glutathione, glutathione s-transferase and catalase values in the permanent-MCAO rats have been reduced, that may make plasma membranes vulnerable to peroxide and attacks by extra free radicals. Consequently, we observed raised level of TBARS, followed by exhausted rates of reduced glutathione; glutathione-s transferase and catalase in permanent-MCAO group whereas after-treatment with MLT-SLNs effectively reversed these effects as compared to MLT dispersion ($p < 0.05$), which is compatible with earlier findings whereas antioxidants were utilized as a therapy in investigational ischemic stroke induced models [62]. MLT-SLNs increased the expression of NRf2 resulting in reduced oxidative stress and ultimately decreased neuroinflammation by effectively reducing the expression of NFKB/IKKβ pathway constituents and other inflammatory markers (TNF-α) efficiently as compare to MLT dispersion, due to significantly improved the distribution of MLT in brain. Moreover, our findings are consistent with the reported findings which mentioned the significant value of NRf2 in the brain inflammation. The stimulation of NRf2 saved brain inflammation while hindrance of NRf2 intensified pro-inflammatory factors and cerebral inflammation in numerous cerebral ischemic and further neuroimpairment related-models [69–73].

3.8. Effect of MLT-SLNs on p-MCAO induced inflammatory markers

Inflammatory markers like tumor necrosis factor-alpha and Interleukin-1 beta that binds to individual receptors activated successive stimulation of downstream molecules like SEK1, JNK and ASK1. This causes nuclear translocation of *p*-NFkB and proteasomal
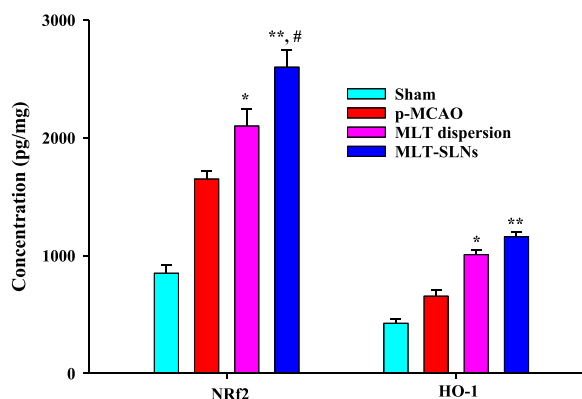
Fig. 6. Effects of MLT-SLNs on the concentrations of NRf2 and HO-1 in rat brain by ELISA analysis. The data are displayed as mean ± standard deviation, and statistical significance was analyzed by one-way ANOVA (n = 3). *$p < 0.05$ and **$p < 0.01$ against *p*-MCAO, and #$p < 0.05$ against MLT dispersion.

dependent IκB dissociation, which together activate inflammatory transcription factors like COX-2 and NOS2 [74]. These proteins like *p*-NFkB were highly increased in enzyme linked immunosorbent assay results in the cerebral ischemic rats and the MLT-SLNs post-treatment meaningfully lessened the expression as compared to MLT-dispersion (p value < 0.01 and p value < 0.05 respectively). MLT-SLNs increased the expression of NRf2, resulting in lessened oxidative stress and ultimately decreased neuroinflammation by effectively declining the expression of NFKB/IKKβ pathway constituents and other inflammatory factors (TNF-α) efficiently as compare to MLT dispersion due to significantly improved the distribution of MLT in brain. We then observed the effects of MLT-SLNs on inflammatory-associated markers (Fig. 7). An increase value of tumor necrosis factor alpha might be measured after permanent-MCAO that might be significantly reduced by MLT-SLNs as compared to MLT-dispersion (p value < 0.01 and p value < 0.05 respectively) by ELISA findings. Moreover, all above previous findings mentioned elaborates the anti-oxidant and anti-inflammatory potential of MLT-SLNs that plays a noteworthy role in the inhibition of apoptosis and neurodegeneration in the treatment of ischemic brain injury.

A BBB model and inhibitors connected with the signaling pathways will be used in our future work to further study the underlying mechanism of the MLT-SLNs. It is noteworthy that MLT-SLNs displayed excellent neuroprotective effects in this study as compared to MLT-dispersion. In a nutshell, we suggest that MLT-SLNs can be used as a hopeful neuroprotective drug delivery system for the treatment of ischemic stroke.

3.9. Estimation of adverse effects

Since certain changes in liver enzymes are documented to occur during an ischemic stroke [75], this is why the outcome of MLT dispersion and MLT-SLNs on liver function were also assessed. Notably increased ALT and AST levels observed in *p*-MCAO as compared with sham operated group. The MLT-SLNs meaningfully reduce the levels of (ALT, AST) (p < 0.01) as compared to MLT dispersion (Table 3). It was establish that MLT uses its hepatoprotective outcomes by activating the signaling pathway NRf2/HO-1 via phosphatidylinositide 3-kinase (PI3K)/protein kinase B (Akt) pathway [76]. In the case of MLT-SLNs, decreased hepatotoxicity could be due to MLT hepatoprotective activity and targeted delivery of prepared MLT-SLNs, as well as increased delivery of MLT-SLNs in the brain, consistent with all above previous findings. These outcomes confirmed that the developed system is safe, biocompatible and displays a more favored delivery to the targeted area than the free MLT. Further studies are strongly encouraged to investigate hepatoprotective function of MLT-SLNs.

4. Conclusion

The emergence of lipid nanoparticles as a multipurpose nanomedicine for a variety of drug delivery systems. To achieve optimum therapeutic outcomes in ischemic stroke, efficient and accurate brain delivery of MLT is required. MLT-SLNs have been successfully developed in this study to enhance its brain delivery in cerebral ischemia. In this research, we investigated the ability of SLNs prepared with biocompatible and biodegradable constituents to overwhelmed the restricted distribution of MLT to the brain. MLN-SLNs allowed high drug incorporation (~92%) with significantly improved aqueous solubility of MLT. MLT-SLNs substantially improved MLT brain deposition, combined with increased *in vivo* neuroprotective activity relative to MLT dispersion. These neuroprotective effects may be mediated by its action on the suppression of proinflammatory cytokines and multiple inflammatory mediators such as NF-kb and tumor necrosis factor-alpha as well as the upregulation of anti-oxidant proteins by activating the endogenous antioxidant NRf2. These results evidently show that MLT-SLNs might be a hopeful neuroprotective pharmaceutical formulation for the treatment of cerebral ischemic injury, mainly by stimulating the NRf2/HO-1 signaling pathway. Though, wide examination is further needed to define the underlying defensive mechanisms of MLT-SLNs. MLT-SLNs could be of unlimited potential to improve MLT therapeutic potential and reduce the danger of brain injury in cerebral ischemic stroke. SLNs-mediated brain drug distribution proposes a hopeful approach that will open up novel outlook for the management of neurological ailments. The prepared carrier method can prove to be an effective
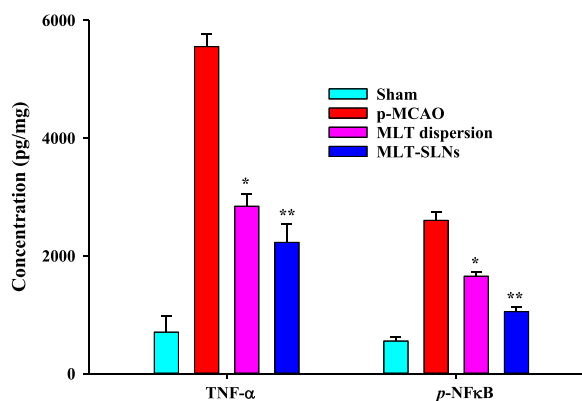
Fig. 7. Suppression of permanent-MCAO induced inflammatory markers (TNF-alpha and *p*-NFκB) by MLT-SLNs in rat cortex quantified by ELISA. The data are expressed as mean ± standard deviation, and statistical significance was analyzed by one-way ANOVA (n = 3). **$p < 0.01$ and *$p < 0.05$ against *p*-MCAO group.

Table 3
Effect of MLT-SLNs treatment on plasma ALT and AST levels in rats.

Groups	ALT (IU/L)	AST (IU/L)
Sham	47.0 ± 2.8	220.0 ± 14.1
p-MCAO	126.5 ± 3.5	532.5 ± 24.7
MLT dispersion	$55.5 \pm 2.1^{**}$	$214.5 \pm 7.8^{**}$
MLT-SLNs	$49.5 \pm 2.1^{**}$	$195.0 \pm 7.1^{**}$

Abbreviations: ALT; alanine aminotransferase, AST; aspartate aminotransferase.
Data are expressed as mean $\pm$ S.D. (n = 3). $^{**}p < 0.01$ against p-MCAO group.

transition of MLT-SLNs from lab to clinical practice, and can be further discovered for the management of other horrible disease situations such as cancer. To sum up, the results of this study in relative to MLT-SLNs, delivered a convincing argument for use of this strategy in the treatment of cerebral ischemic stroke.

Author contribution statement

Saba Sohail, M Phil: Performed the experiments; Analyzed and interpreted the data.
Fawad Ali Shah, PhD: Performed the experiments; Contributed reagents, materials, analysis tools or data.
Shahiq uz Zaman, PhD; Imran Malik, M Phil: Analyzed and interpreted the data.
Ali Almari, PhD: Analyzed and interpreted the data; Wrote the paper.
Saifoor Ahmad Khan, M Phil: Performed the experiments.
Abir Abdullah Alamro, PhD: Contributed reagents, materials, analysis tools or data; Wrote the paper.
Alam Zeb, PhD; Fakhar Ud Din, PhD: Conceived and designed the experiments; Wrote the paper.

Data availability statement

Data included in article/supp. material/referenced in article.

Additional information

No additional information is available for this paper.

Declaration of competing interest

The authors declare that they have no known competing financial interests or personal relationships that could have appeared to influence the work reported in this paper.

Acknowledgements

References

[1] E.S. Donkor, Stroke in the 21(st) century: a snapshot of the burden, epidemiology, and quality of life, Stroke research and treatment 2018 (2018), 3238165.
[2] K.P. Doyle, R.P. Simon, M.P. Stenzel-Poore, Mechanisms of ischemic brain damage, Neuropharmacology 55 (2008) 310–318.
[3] F. Liu, L.D. McCullough, Middle cerebral artery occlusion model in rodents: methods and potential pitfalls, J. Biomed. Biotechnol. 2011 (2011), 464701.
[4] O.-N. Bae, K. Serfozo, S.-H. Baek, K.Y. Lee, A. Dorrance, W. Rumbeiha, S.D. Fitzgerald, M.U. Farooq, B. Naravelta, A. Bhatt, A. Majid, Safety and efficacy evaluation of carnosine, an endogenous neuroprotective agent for ischemic stroke, Stroke 44 (2013) 205–212.
[5] A.R. Green, A. Shuaib, Therapeutic strategies for the treatment of stroke, Drug Discov. Today 11 (2006) 681–693.
[6] C. Venegas, J.A. García, G. Escames, F. Ortiz, A. López, C. Doerrier, L. García-Corzo, L.C. López, R.J. Reiter, D. Acuña-Castroviejo, Extrapineal melatonin: analysis of its subcellular distribution and daily fluctuations, J. Pineal Res. 52 (2012) 217–227.
[7] E. Ramos, P. Patiño, R.J. Reiter, E. Gil-Martín, J. Marco-Contelles, E. Parada, C. de Los Rios, A. Romero, J. Egea, Ischemic brain injury: new insights on the protective role of melatonin, Free Radic. Biol. Med. 104 (2017) 32–53.
[8] F.A. Shah, A. Zeb, T. Ali, T. Muhammad, M. Faheem, S.I. Alam, K. Saeed, P.O. Koh, K.W. Lee, M.O. Kim, Identification of proteins differentially expressed in the striatum by melatonin in a middle cerebral artery occlusion rat model-a proteomic and in silico approach, Front. Neurosci. 12 (2018) 888.
[9] A. Sakellaropoulou, A. Siamidi, M. Vlachou, Melatonin/cyclodextrin inclusion complexes: a review, Molecules 27 (2022) 445.
[10] F.N. Siahdasht, N. Farhadian, M. Karimi, L. Hafizi, Enhanced Delivery of Melatonin Loaded Nanostructured Lipid Carriers during in Vitro Fertilization: NLC Formulation, Optimization and IVF Efficacy, vol. 10, Royal Society of Chemistry Advances, 2020, pp. 9462–9475.
[11] N.G. Harpsøe, L.P.H. Andersen, I. Gögenur, J. Rosenberg, Clinical pharmacokinetics of melatonin: a systematic review, Eur. J. Clin. Pharmacol. 71 (2015) 901–909.

[12] E.R. de Oliveira Junior, T.L. Nascimento, M.A. Salomão, A.C.G. da Silva, M.C. Valadares, E.M. Lima, Increased nose-to-brain delivery of melatonin mediated by polycaprolactone nanoparticles for the treatment of glioblastoma, Pharmaceut. Res. 36 (2019) 131.

[13] Y. Li, X. Zhao, Y. Zu, L. Wang, W. Wu, Y. Deng, C. Zu, Y. Liu, Melatonin-loaded silica coated with hydroxypropyl methylcellulose phthalate for enhanced oral bioavailability: preparation, and in vitro-in vivo evaluation, Eur. J. Pharm. Biopharm. 112 (2017) 58–66.

[14] E.A. Bseiso, S.A. Abd El-Aal, M. Nasr, O.A. Sammour, N.A. Abd El Gawad, Intranasally administered melatonin core-shell polymeric nanocapsules: a promising treatment modality for cerebral ischemia, Life Sci. 306 (2022), 120797.

[15] E.A. Bseiso, S.A. AbdEl-Aal, M. Nasr, O.A. Sammour, N.A.A. El Gawad, Nose to brain delivery of melatonin lipidic nanocapsules as a promising post-ischemic neuroprotective therapeutic modality, Drug Deliv. 29 (2022) 2469–2480.

[16] A. Priprem, J.R. Johns, S. Limsitthichaikoon, W. Limphirat, P. Mahakunakorn, N.P. Johns, Intranasal melatonin nanoniosomes: pharmacokinetic, pharmacodynamic and toxicity studies, Ther. Deliv. 8 (2017) 373–390.

[17] M. Gul, F.A. Shah, N.-u. Sahar, I. Malik, F.u. Din, S.A. Khan, W. Aman, H.-I. Choi, C.-W. Lim, H.-Y. Noh, J.-S. Noh, A. Zeb, J.-K. Kim, Formulation optimization, in vitro and in vivo evaluation of agomelatine-loaded nanostructured lipid carriers for augmented antidepressant effects, Colloids Surf. B Biointerfaces 216 (2022), 112537.

[18] A. Zeb, J.-H. Cha, A.R. Noh, O.S. Qureshi, K.-W. Kim, Y.-H. Choe, D. Shin, F.A. Shah, A. Majid, O.-N. Bae, J.-K. Kim, Neuroprotective effects of carnosine-loaded elastic liposomes in cerebral ischemia rat model, J Pharm Inv 1 (2019) 1–9.

[19] N. Khan, F.A. Shah, I. Rana, M.M. Ansari, F.u. Din, S.Z.H. Rizvi, W. Aman, G.-Y. Lee, E.-S. Lee, J.-K. Kim, A. Zeb, Nanostructured lipid carriers-mediated brain delivery of carbamazepine for improved in vivo anticonvulsant and anxiolytic activity, Int. J. Pharm. 577 (2020), 119033.

[20] M. Yasir, U.V.S. Sara, I. Chauhan, P.K. Gaur, A.P. Singh, D. Puri A, Solid lipid nanoparticles for nose to brain delivery of donepezil: formulation, optimization by Box–Behnken design, in vitro and in vivo evaluation, Artificial Cells, Nanomedicine, and Biotechnology 46 (2018) 1838–1851.

[21] M. Yasir, I. Chauhan, A. Zafar, M. Verma, K.M. Noorulla, A.J. Tura, N.K. Alruwaili, M.J. Haji, D. Puri, W.G. Gobena, D.D. Dalecha, U.V.S. Sara, N. Kumar, Buspirone loaded solid lipid nanoparticles for amplification of nose to brain efficacy: formulation development, optimization by Box-Behnken design, in-vitro characterization and in-vivo biological evaluation, J. Drug Deliv. Sci. Technol. 61 (2021), 102164.

[22] M. Yasir, U.V. Sara, Solid lipid nanoparticles for nose to brain delivery of haloperidol: in vitro drug release and pharmacokinetics evaluation, Acta Pharm. Sin. B 4 (2014) 454–463.

[23] S.Z.H. Rizvi, F.A. Shah, N. Khan, I. Muhammad, K.H. Ali, M.M. Ansari, F. ud Din, O.S. Qureshi, K.-W. Kim, Y.-H. Choe, Simvastatin-loaded solid lipid nanoparticles for enhanced anti-hyperlipidemic activity in hyperlipidemia animal model, Int. J. Pharm. 560 (2019) 136–143.

[24] O.S. Qureshi, H.-S. Kim, A. Zeb, J.-S. Choi, H.-S. Kim, J.-E. Kwon, M.-S. Kim, J.-H. Kang, C. Ryou, J.-S. Park, Sustained release docetaxel-incorporated lipid nanoparticles with improved pharmacokinetics for oral and parenteral administration, J. Microencapsul. 34 (2017) 250–261.

[25] F.u. Din, A. Zeb, K.U. Shah, R. Zia ur, Development, in-vitro and in-vivo evaluation of ezetimibe-loaded solid lipid nanoparticles and their comparison with marketed product, J. Drug Deliv. Sci. Technol. 51 (2019) 583–590.

[26] F. Noori Siahdasht, N. Farhadian, M. Karimi, L. Hafizi, Enhanced delivery of melatonin loaded nanostructured lipid carriers during in vitro fertilization: NLC formulation, optimization and IVF efficacy, RSC Adv. 10 (2020) 9462–9475.

[27] A. Zeb, O.S. Qureshi, H.-S. Kim, J.-H. Cha, H.-S. Kim, J.-K. Kim, Improved skin permeation of methotrexate via nanosized ultradeformable liposomes, Int. J. Nanomed. 11 (2016) 3813–3824.

[28] F.A. Shah, G. Liu, L.T. Al Kury, A. Zeb, P.-O. Koh, M. Abbas, T. Li, X. Yang, F. Liu, Y. Jiang, S. Li, Melatonin protects MCAO-induced neuronal loss via NR2A mediated prosurvival pathways, Front. Pharmacol. 10 (2019) 297.

[29] F.A. Shah, S.-A. Gim, M.-O. Kim, P.-O. Koh, Proteomic identification of proteins differentially expressed in response to resveratrol treatment in middle cerebral artery occlusion stroke model, J. Vet. Med. Sci. 76 (2014) 1367–1374.

[30] F.A. Shah, S.-A. Gim, J.-H. Sung, S.-J. Jeon, M.-O. Kim, P.-O. Koh, Identification of proteins regulated by curcumin in cerebral ischemia, J. Surg. Res. 201 (2016) 141–148.

[31] D.-J. Park, F.-A. Shah, P.-O. Koh, Quercetin attenuates neuronal cells damage in a middle cerebral artery occlusion animal model, J. Vet. Med. Sci. 80 (2018) 676–683.

[32] M. Imran, L.T. Al Kury, H. Nadeem, F.A. Shah, M. Abbas, S. Naz, A.U. Khan, S. Li, Benzimidazole containing acetamide derivatives attenuate neuroinflammation and oxidative stress in ethanol-induced neurodegeneration, Biomolecules 10 (2020).

[33] L.T. Al Kury, A. Zeb, Z.U. Abidin, N. Irshad, I. Malik, A.M. Alvi, A.A.K. Khalil, S. Ahmad, M. Faheem, A.U. Khan, F.A. Shah, S. Li, Neuroprotective effects of melatonin and celecoxib against ethanol-induced neurodegeneration: a computational and pharmacological approach, Drug Des. Dev. Ther. 13 (2019) 2715–2727.

[34] J.V. Natarajan, C. Nugraha, X.W. Ng, S. Venkatraman, Sustained-release from nanocarriers: a review, J. Contr. Release 193 (2014) 122–138.

[35] X. Dong, R. Mumper, The metabolism of fatty alcohols in lipid nanoparticles by alcohol dehydrogenase, Drug Dev. Ind. Pharm. 32 (2006) 973–980.

[36] C. Tapeinos, M. Battaglini, G. Ciofani, Advances in the design of solid lipid nanoparticles and nanostructured lipid carriers for targeting brain diseases, J. Contr. Release 264 (2017) 306–332.

[37] Y. Zheng, M. Zheng, Z. Ma, B. Xin, R. Guo, X. Xu, 8 - sugar fatty acid esters, in: Ahmad (Ed.), Polar Lipids, Elsevier2015, pp. 215-243.

[38] T. Schmidts, D. Dobler, C. Nissing, F. Runkel, Influence of hydrophilic surfactants on the properties of multiple W/O/W emulsions, J. Colloid Interface Sci. 338 (2009) 184–192.

[39] A.B. Etame, C.A. Smith, W.C. Chan, J.T. Rutka, Design and potential application of PEGylated gold nanoparticles with size-dependent permeation through brain microvasculature, Nanomed. Nanotechnol. Biol. Med. 7 (2011) 992–1000.

[40] A.R. Neves, J.F. Queiroz, S. Reis, Brain-targeted delivery of resveratrol using solid lipid nanoparticles functionalized with apolipoprotein E, J. Nanobiotechnol. 14 (2016) 27–38.

[41] D. Pandita, S. Kumar, N. Poonia, V. Lather, Solid lipid nanoparticles enhance oral bioavailability of resveratrol, a natural polyphenol, Food Res. Int. 62 (2014) 1165–1174.

[42] P.R. Lockman, J.M. Koziara, R.J. Mumper, D.D. Allen, Nanoparticle surface charges alter blood–brain barrier integrity and permeability, J. Drug Target. 12 (2004) 635–641.

[43] N. Mosallaei, M.R. Jaafari, M.Y. Hanafi-Bojd, S. Golmohammadzadeh, B. Malaekeh-Nikouei, Docetaxel-loaded solid lipid nanoparticles: preparation, characterization, in vitro, and in vivo evaluations, J. Pharmaceut. Sci. 102 (2013) 1994–2004.

[44] V. Venkateswarlu, K. Manjunath, Preparation, characterization and in vitro release kinetics of clozapine solid lipid nanoparticles, Int. J. Food Eng. 95 (2004) 627–638.

[45] Q. Lv, A. Yu, Y. Xi, H. Li, Z. Song, J. Cui, F. Cao, G. Zhai, Development and evaluation of penciclovir-loaded solid lipid nanoparticles for topical delivery, Int. J. Pharm. 372 (2009) 191–198.

[46] M. Sabzichi, N. Samadi, J. Mohammadian, H. Hamishehkar, M. Akbarzadeh, O. Molavi, Sustained release of melatonin: a novel approach in elevating efficacy of tamoxifen in breast cancer treatment, Colloids Surf., B 145 (2016) 64–71.

[47] N. Dudhipala, K. Veerabrahma, Improved anti-hyperlipidemic activity of rosuvastatin calcium via lipid nanoparticles: pharmacokinetic and pharmacodynamic evaluation, Eur. J. Pharm. Biopharm. 110 (2017) 47–57.

[48] M. Liu, J. Dong, Y. Yang, X. Yang, H. Xu, Characterization and release of triptolide-loaded poly (D, L-lactic acid) nanoparticles, Eur. Polym. J. 41 (2005) 375–382.

[49] X. Huang, G. Alva, L. Liu, G. Fang, Microstructure and thermal properties of cetyl alcohol/high density polyethylene composite phase change materials with carbon fiber as shape-stabilized thermal storage materials, Appl. Energy 200 (2017) 19–27.

[50] H. Valizadeh, A. Nokhodchi, N. Qarakhani, P. Zakeri-Milani, S. Azarmi, D. Hassanzadeh, R. Löbenberg, Physicochemical characterization of solid dispersions of indomethacin with PEG 6000, Myrj 52, lactose, sorbitol, dextrin, and Eudragit E100, Drug Dev. Ind. Pharm. 30 (2004) 303–317.

[51] A.-R.M. El-Helw, U.A. Fahmy, Improvement of fluvastatin bioavailability by loading on nanostructured lipid carriers, Int. J. Nanomed. 10 (2015) 5797–5804.

[52] A. zur Mühlen, C. Schwarz, W. Mehnert, Solid lipid nanoparticles (SLN) for controlled drug delivery–drug release and release mechanism, Eur. J. Pharm. Biopharm. 45 (1998) 149–155.

[53] O.S. Qureshi, A. Zeb, M. Akram, M.-S. Kim, J.-H. Kang, H.-S. Kim, A. Majid, I. Han, S.-Y. Chang, O.-N. Bae, Enhanced acute anti-inflammatory effects of CORM-2-loaded nanoparticles via sustained carbon monoxide delivery, Eur. J. Pharm. Biopharm. 108 (2016) 187–195.

[54] F.A. Shah, L.A. Kury, T. Li, A. Zeb, P.O. Koh, F. Liu, Q. Zhou, I. Hussain, A.U. Khan, Y. Jiang, S. Li, Polydatin attenuates neuronal loss via reducing neuroinflammation and oxidative stress in rat MCAO models, Front. Pharmacol. 10 (2019) 663.

[55] T. Fukuta, T. Ishii, T. Asai, N. Oku, Applications of liposomal drug delivery systems to develop neuroprotective agents for the treatment of ischemic stroke, Biol. Pharm. Bull. 42 (2019) 319–326.

[56] I.P. Kaur, R. Bhandari, S. Bhandari, V. Kakkar, Potential of solid lipid nanoparticles in brain targeting, J. Contr. Release 127 (2008) 97–109.

[57] H.L. Wong, N. Chattopadhyay, X.Y. Wu, R. Bendayan, Nanotechnology applications for improved delivery of antiretroviral drugs to the brain, Adv. Drug Deliv. Rev. 62 (2010) 503–517.

[58] C. Saraiva, C. Praça, R. Ferreira, T. Santos, L. Ferreira, L. Bernardino, Nanoparticle-mediated brain drug delivery: overcoming blood–brain barrier to treat neurodegenerative diseases, J. Contr. Release 235 (2016) 34–47.

[59] P. Blasi, S. Giovagnoli, A. Schoubben, M. Ricci, C. Rossi, Solid lipid nanoparticles for targeted brain drug delivery, Adv. Drug Deliv. Rev. 59 (2007) 454–477.

[60] A. Ali, F.A. Shah, A. Zeb, I. Malik, A.M. Alvi, L.T. Alkury, S. Rashid, I. Hussain, N. Ullah, A.U. Khan, P.O. Koh, S. Li, NF-κB inhibitors attenuate MCAO induced neurodegeneration and oxidative stress-A reprofiling approach, Front. Mol. Neurosci. 13 (2020) 33.

[61] N. Watson, T. Diamandis, C. Gonzales-Portillo, S. Reyes, C.V. Borlongan, Melatonin as an antioxidant for stroke neuroprotection, Cell Transplant. 25 (2016) 883–891.

[62] R. Shirley, E.N.J. Ord, L.M. Work, Oxidative stress and the use of antioxidants in stroke, Antioxidants 3 (2014) 472–501.

[63] B. Prathipati, P. Rohini, P.K. Kola, R.C.S. Reddy Danduga, Neuroprotective effects of curcumin loaded solid lipid nanoparticles on homocysteine induced oxidative stress in vascular dementia, Current Research in Behavioral Sciences 2 (2021), 100029.

[64] S.A. Reisman, L.M. Aleksunes, C.D. Klaassen, Oleanolic acid activates Nrf2 and protects from acetaminophen hepatotoxicity via Nrf2-dependent and Nrf2-independent processes, Biochem. Pharmacol. 77 (2009) 1273–1282.

[65] H. Liu, W. Chen, P. Lu, Y. Ma, X. Liang, Y. Liu, Ginsenoside Rg1 attenuates the inflammation and oxidative stress induced by diabetic nephropathy through regulating the PI3K/AKT/FOXO3 pathway, Ann. Transl. Med. 9 (2021) 1789.

[66] G. Ashabi, L. Khalaj, F. Khodagholi, M. Goudarzvand, A. Sarkaki, Pre-treatment with metformin activates Nrf2 antioxidant pathways and inhibits inflammatory responses through induction of AMPK after transient global cerebral ischemia, Metab. Brain Dis. 30 (2015) 747–754.

[67] B. Sun, S. Yang, S. Li, C. Hang, Melatonin upregulates nuclear factor erythroid-2 related factor 2 (Nrf2) and mediates mitophagy to protect against early brain injury after subarachnoid hemorrhage, Med Sci Monit 24 (2018) 6422–6430.

[68] T. Ali, S.U. Rehman, F.A. Shah, M.O. Kim, Acute dose of melatonin via Nrf2 dependently prevents acute ethanol-induced neurotoxicity in the developing rodent brain, J. Neuroinflammation 15 (2018) 119.

[69] E.H. Kobayashi, T. Suzuki, R. Funayama, T. Nagashima, M. Hayashi, H. Sekine, N. Tanaka, T. Moriguchi, H. Motohashi, K. Nakayama, M. Yamamoto, Nrf2 suppresses macrophage inflammatory response by blocking proinflammatory cytokine transcription, Nat. Commun. 7 (2016), 11624.

[70] J. Yang, J. Su, F. Wan, N. Yang, H. Jiang, M. Fang, H. Xiao, J. Wang, J. Tang, Tissue kallikrein protects against ischemic stroke by suppressing TLR4/NF-κB and activating Nrf2 signaling pathway in rats, Exp. Ther. Med. 14 (2017) 1163–1170.

[71] D. Liu, J. Xue, Y. Liu, H. Gu, X. Wei, W. Ma, W. Luo, L. Ma, S. Jia, N. Dong, J. Huang, Y. Wang, Z. Yuan, Inhibition of NRF2 signaling and increased reactive oxygen species during embryogenesis in a rat model of retinoic acid-induced neural tube defects, Neurotoxicology 69 (2018) 84–92.

[72] B.L. Ya, Q. Liu, H.F. Li, H.J. Cheng, T. Yu, L. Chen, Y. Wang, L.L. Yuan, W.J. Li, W.Y. Liu, B. Bai, Uric acid protects against focal cerebral ischemia/reperfusion-induced oxidative stress via activating Nrf2 and regulating neurotrophic factor expression, Oxid. Med. Cell. Longev. (2018), 6069150, 2018.

[73] G. Bahn, J.S. Park, U.J. Yun, Y.J. Lee, Y. Choi, J.S. Park, S.H. Baek, B.Y. Choi, Y.S. Cho, H.K. Kim, J. Han, J.H. Sul, S.H. Baik, J. Lim, N. Wakabayashi, S.H. Bae, J. W. Han, T.V. Arumugam, M.P. Mattson, D.G. Jo, NRF2/ARE pathway negatively regulates BACE1 expression and ameliorates cognitive deficits in mouse Alzheimer's models, Proc Natl Acad Sci U S A 116 (2019) 12516–12523.

[74] T.G. Davies, W.E. Wixted, J.E. Coyle, C. Griffiths-Jones, K. Hearn, R. McMenamin, D. Norton, S.J. Rich, C. Richardson, G. Saxty, H.M. Willems, A.J. Woolford, J. E. Cottom, J.P. Kou, J.G. Yonchuk, H.G. Feldser, Y. Sanchez, J.P. Foley, B.J. Bolognese, G. Logan, P.L. Podolin, H. Yan, J.F. Callahan, T.D. Heightman, J.K. Kerns, Monoacidic inhibitors of the kelch-like ECH-associated protein 1: nuclear factor erythroid 2-related factor 2 (KEAP1:NRF2) protein-protein interaction with high cell potency identified by fragment-based discovery, J. Med. Chem. 59 (2016) 3991–4006.

[75] A. Muscari, A. Collini, E. Fabbri, M. Giovagnoli, C. Napoli, V. Rossi, L. Vizioli, A. Bonfiglioli, D. Magalotti, G. Puddu, M. Zoli, Changes in liver enzymes and bilirubin during ischemic stroke: mechanisms and possible significance, BioMed Central Neurology 14 (2014) 122–131.

[76] Z. Ahmadi, M. Ashrafizadeh, Melatonin as a potential modulator of Nrf2, Fund. Clin. Pharmacol. 34 (2020) 11–19.